PEEK Oligomers: A Model for the Polymer Physical Behavior. 2. Structure and Thermal Behavior of Linear Monodisperse Oligomers

Alain Jonas*,[1] and Roger Legras

Laboratoire de Physique et de Chimie des Hauts Polymères, Université Catholique de Louvain, Place Croix du Sud, 1, B-1348 Louvain-la-Neuve, Belgium

Rolf Scherrenberg and Harry Reynaers

Laboratory for Macromolecular Structural Chemistry, Katholieke Universiteit Leuven, Celestijnenlaan, 200F, B-3001 Heverlee, Belgium

Received March 30, 1992; Revised Manuscript Received October 14, 1992

ABSTRACT: The thermal and structural properties of monodisperse linear poly(oxy-1,4-phenyloxy-1,4-phenylenecarbonyl-1,4-phenylene) (PEEK) oligomers have been investigated by differential scanning calorimetry, optical microscopy, and wide-angle and small-angle X-ray scattering. The complex melting, observed for the longest oligomers, is related to variations in the relative placement of the ether and ketone bridges of the chains in the lamellae (eclipsed and staggered lamellae). Chain packing is discussed in terms of chain staggering, and appropriate conclusions are drawn concerning the variations of the polymer unit cell dimensions with crystallization temperature. Two different types of spherulites have been detected for the longest oligomer; these are shown to result from differences in the preferred main orientation of the (100) planes of the lamellae.

Introduction

In the previous paper of this series,[2] the synthesis of linear monodisperse oligomers of poly(oxy-1,4-phenyleneoxy-1,4-phenylenecarbonyl-1,4-phenylene) (PEEK) has been described. Using various spectroscopic techniques, the chemical structures of these compounds were confirmed. In the present paper, the thermal behavior of the oligomers will be studied in relation to their crystalline packing, in order to gain insight into the crystalline structure of the polymer itself.

The crystallographic studies of PEEK reported in the literature[3-7] all agree in considering the ether and ketone bridges as crystallographically equivalent. The PEEK space group (*Pbcn*) is similar to the one of poly(phenylene oxide); actually it was shown that the space groups of various polymers of the poly(aryl ether ketone) family, differing in their relative amounts of ether to ketone bridges, are all similar, except of course for the exact values of the lattice parameters.[8]

A representation of the PEEK unit cell is given in Figure 1: a is the dimension of the unit cell perpendicular to the zigzag planes (b–c planes), and c is as usual the lattice parameter in the chain axis direction. The tilt angle of the phenyl groups relative to the (100) planes is reported to be on the order of 40°.

The question of the isomorphic placement of ketone and ether bridges in the PEEK lamellae is still unresolved. A recent theoretical study[9] reports on the energy of interaction between the polymer chains as a function of the relative placement of the ether and ketone bridges. The authors concluded that small differences exist for various alignments of the bridges; the observed variations of the unit cell dimensions with crystallization temperature were attributed to the evolution of the relative placement of the bridges from disordered alignments toward more regular and stable ones. One of the objectives of the present study is to offer new experimental progress with respect to these questions.

An ideal characterization of the oligomer structures requires evidently growth of single crystals large enough

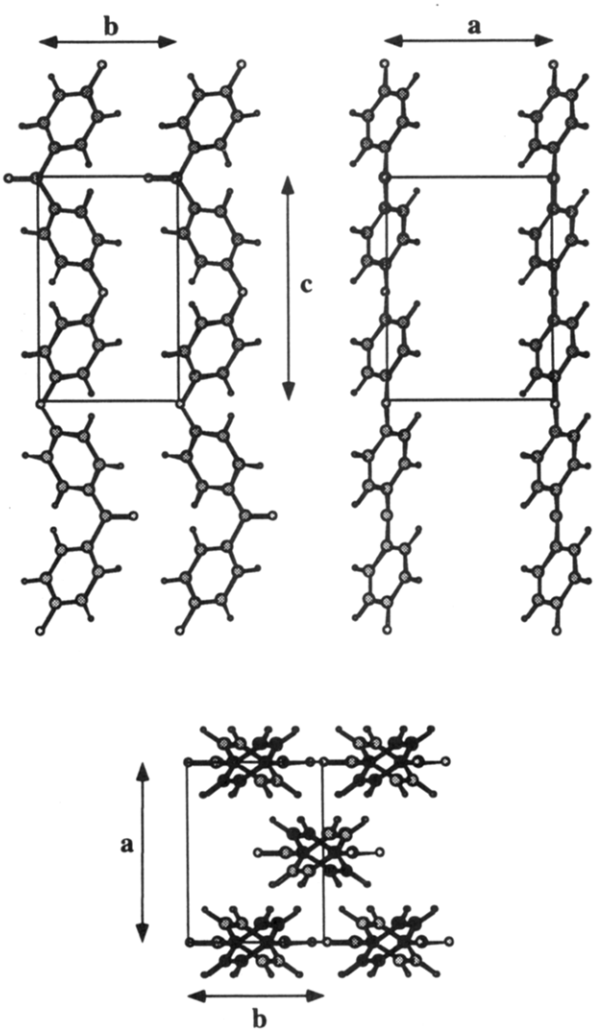

Figure 1. PEEK crystalline unit cell. Due to isomorphic placement of ketone and ether bridges, the c axis is only two-thirds of the monomer repeating unit. Upper left: projection on (100). Upper right: projection on (010). Below: view along the c axis.

0024-9297/93/2226-0526$04.00/0

Table I
Nomenclature and Extended Length of the Oligomers

compound[a]	nomenclature	extended length (nm)
ΦOΦOΦCOΦOΦOΦ	EEKEE	3.10
ΦOΦOΦCOΦ(OΦOΦCOΦ)$_1$OΦOΦ	EEK(EEK)$_1$EE	4.57
ΦOΦOΦCOΦ(OΦOΦCOΦ)$_2$OΦOΦ	EEK(EEK)$_2$EE	6.04
FΦCOΦ(OΦOΦCOΦ)$_1$F	FK(EEK)$_1$F	2.72
FΦCOΦ(OΦOΦCOΦ)$_2$F	FK(EEK)$_2$F	4.19
FΦCOΦ(OΦOΦCOΦ)$_3$F	FK(EEK)$_3$F	5.66
FΦCOΦ(OΦOΦCOΦ)$_4$F	FK(EEK)$_4$F	7.13

[a] Φ is the symbol of a para-disubstituted phenyl group, and F stands for fluorine.

to perform an X-ray structure analysis. However, the poor solubility of the longest PEEK oligomers, which are the most interesting ones, renders the growth of such large single crystals very hypothetical. Hence, it was preferred to analyze polycrystallize powders by X-ray diffraction using at once various other complementary techniques which compensate for the loss of information due to the polycrystalline nature of the samples. As will be clarified below, this is only partially true; however, some interesting information could be extracted in any way by this multiplication of sources of information.

The oligomers nomenclature used in this paper is presented in Table I, together with their computed extended chain lengths, as estimated from standard bond angles and lengths and from data published on benzophenone and diphenyl ether.[10] A extensive characterization of these oligomers by differential scanning calorimetry (DSC), optical microscopy (OM), wide-angle X-ray scattering (WAXS), and small-angle X-ray scattering (SAXS) has been performed. A detailed description of the thermal behavior and X-ray characterization of each oligomer can be found elsewhere.[11] In the present paper, the main observations will be summarized and illustrated by selected examples.

Results and Discussion

Results have been obtained on the as-synthesized powders, after recrystallization in *N*-methyl-2-pyrrolidone (NMP) (hereafter denoted as "virgin powders"), as well as on variously heat-treated samples, always starting from the virgin powders.

1. Complex Melting Behavior. 1.1. DSC Experiments. The shortest oligomers (EEKEE, FK(EEK)$_{1-2}$F) exhibit only one melting peak, whatever the crystallization condition. Accordingly, upon cooling these oligomers at −10 °C min^{-1}, a single sharp exothermic crystallization peak is detected. The melting peak temperature location ($T_{m,peak}$) depends slightly on the heating rate, whereas the onset temperature ($T_{m,ons}$) is almost independent of it. Values of these temperatures extrapolated to 0 °C min^{-1} heating rate are given in Table II. As expected for perfect molecular crystals, the extrapolated values for $T_{m,peak}$ and $T_{m,ons}$ are nearly equal. There is a weak effect on chain-end nature on melting enthalpy and temperature. A similar thermal meltint behavior is exhibited by the longest phenoxy-ended oligomer (EEK(EEK)$_2$EE) (Table II). The melting enthalpy of this compound is significantly smaller than that for the shorter oligomers.

By contrast, the EEK(EEK)$_1$EE, FK(EEK)$_3$F, and FK(EEK)$_4$F oligomers exhibit a complex melting behavior with two or three successive reproducible melting peaks. The melting temperatures corresponding to the various crystal populations of these compounds are reported in Table III. We shall detail here only the behavior of EEK(EEK)$_1$EE. Similar behaviors have been observed for the two other oligomers.[11]

Table II
Thermal Properties of PEEK Oligomers Having Only One Melting Peak (Values Extrapolated to 0 °C min^{-1} Scan Rate)

oligomer[a]	$T_{m,ons}$[b] (°C)	$T_{m,peak}$[b] (°C)	ΔH_m[b] (J g^{-1})	$T_{cc,ons}$[c] (°C)	ΔH_{cc}[c] (J g^{-1})
FK(EEK)$_1$F	231.0	231.0	142	214.5	−130
EEKEE	198.3	199.3	131	174.3	−122
FK(EEK)$_2$F	289.7	290.3	143	279.9	−137
EEK(EEK)$_2$EE	278.3	280.4	111	272.3	−102

[a] From shortest to longest. [b] Values measured on virgin powders and extrapolated to 0 °C min^{-1} heating rate. [c] $T_{cc,ons}$ and ΔH_{cc} are the crystallization onset temperature and enthalpy observed when cooling the oligomers from the melt at −10 °C min^{-1}.

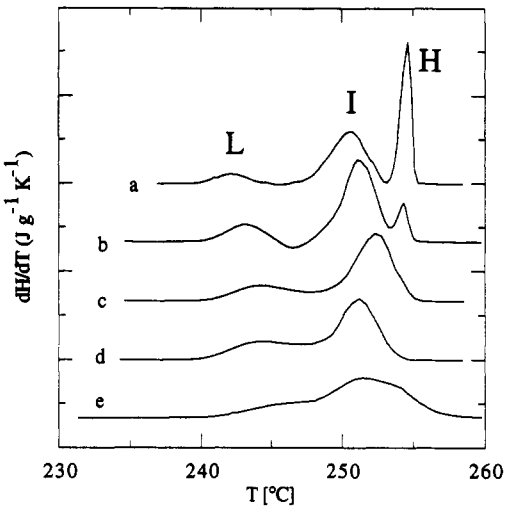

Figure 2. DSC thermograms of the EEK(EEK)$_1$EE virgin powder for scanning rates (a) 2, (b) 5, (c) 10, (d) 20, and (e) 50 °C min^{-1}.

Table III
Peak Melting Temperatures and Crystal Population Nomenclature of PEEK Oligomers Exhibiting Complex Melting

oligomer	lower melting endotherm (°C)	intermediate melting endotherm (°C)	upper melting endotherm (°C)
EEK(EEK)$_1$EE	242–245 (type L)	250–252 (type I)	254–255 (type H)
FK(EEK)$_3$F	292–293.5 (type L$_{F3}$)	306–310 (type I$_{F3}$)	313–314.5 (type H$_{F3}$)
FK(EEK)$_4$F		304–307 (type I$_{F4}$)	320–323 (type H$_{F4}$)

The heating thermograms of the EEK(EEK)$_1$EE virgin powder are shown in Figure 2, for scanning rates between 2 and 50 °C min^{-1}. This sample is initially composed of two crystal populations of different thermal stability, melting respectively in the ranges 242–245 and 250–252 °C. These two populations will be denoted as L (for low-temperature melting) and I (for intermediate-temperature melting). The virgin powder consists roughly of 25% type L and 75% type I crystals. For the slowest heating rates, a new melting peak appears around 254–255 °C, corresponding to the formation of a new crystal type during the scan, called type H (high-temperature melting).

Upon cooling the oligomer from the molten state at −10 °C min^{-1}, a single sharp exothermic crystallization peak is observed ($T_{cc,ons}$ = 234.9 °C, $T_{cc,peak}$ = 232.5 °C, ΔH_{cc} = −107 J g^{-1}). Reheating this new sample at various heating rates (Figure 3) reveals that the dynamic crystallization from the melt results in ~50% type L and ~50% type I crystals. As can be inferred from Figure 3, the type L crystals are able to recrystallize rapidly into type I crystals. This is demonstrated by the presence of a well-defined

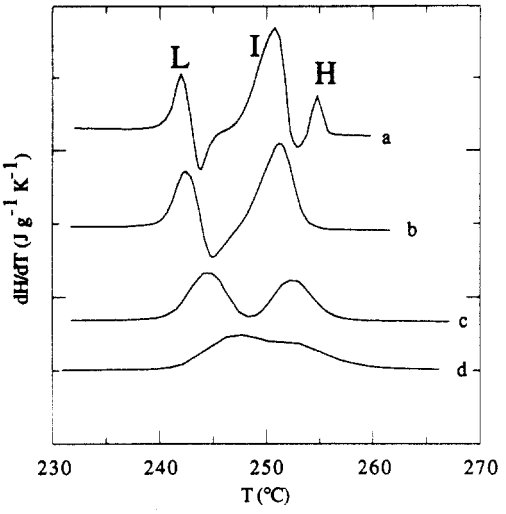

Figure 3. DSC reheating thermograms of EEK(EEK)$_1$EE crystallized from the melt at (a) 10, (b) 20, (c) 50, and (d) 100 °C min^{-1}.

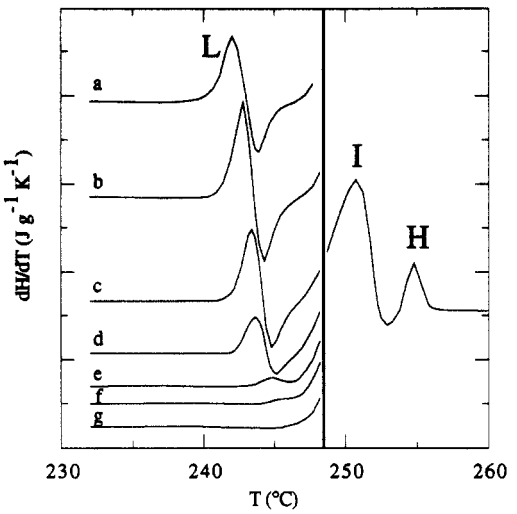

Figure 4. DSC reheating thermograms (10 °C min^{-1}) of EEK(EEK)$_1$EE after dynamic (~50 °C min^{-1}) crystallization from the melt, followed by a 2-min annealing at T_c, before cooling to 200 °C: (a) no annealing, (b) T_c = 240 °C, (c) T_c = 241 °C, (d) T_c = 242 °C, (e) T_c = 242.7 °C, (f) T_c = 243.5 °C, (g) T_c = 245 °C. Above ~247 °C (thick vertical line), the thermograms are all equal; the DSC traces were thus not redrawn for each sample.

exothermic peak between the melting endotherms of the two crystal types; the recrystallization is suppressed only for scanning rates of 50 °C min^{-1} and higher. Due to simultaneous crystallization into type I crystals, the melting endotherm of the type L crystals is reduced for slow scanning rates as compared to its unperturbed value obtained at 50 °C min^{-1}.

Complementary experiments were performed to clarify the L-to-I reorganization phenomenon. Various samples were dynamically crystallized at ~50 °C min^{-1} from the melt, then heated to T_c during 2 min (240 °C < T_c < 245 °C), and finally rapidly cooled to 200 °C. Subsequent 10 °C min^{-1} heating scans are shown in Figure 4. As T_c increases, the type L melting endotherm is shifted upward, while its relative magnitude describes a peaked curve as a function of T_c. All the type L crystals, melting at a temperature lower than T_c, have been converted to type I crystals during the 2-min annealing. In the subsequent heating scan, the melting of the remaining type L crystal fraction only starts from T_c, and the melting endotherm is delayed; the concomitant recrystallization exotherm is also delayed (because of nucleation and growth kinetics),

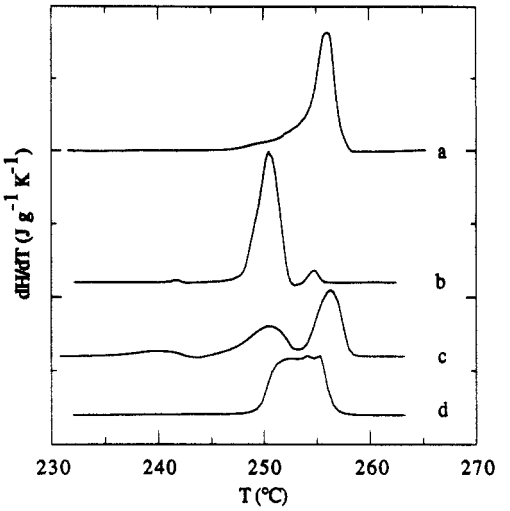

Figure 5. DSC thermograms (10 °C min^{-1}) of EEK(EEK)$_1$EE: (a) after 12 h of crystallization from the molten state, at 250.5 °C; (b) after 30 min of crystallization from the molten state, at 241.6 °C; (c) after 10 min of annealing at 253 °C of the virgin powder; (d) after 10 min of annealing at 246 °C of the virgin powder.

and the net heat flux is displaced toward higher temperatures. By using this procedure, it is found that type L crystals actually melt between 238 and 243.5 °C when measured at 10 °C min^{-1}.

The I-to-H reorganization process was also studied by annealing the EEK(EEK)$_1$EE virgin powder at 253 °C, above the type I crystal's melting temperature but below the type H crystal's melting temperature. Contrary to the L-to-I reorganization, this second process is slow. Figure 5c shows the heating thermogram of a sample maintained 10 min at 253 °C before cooling; a mixture of mainly type H and type I crystals is obtained, the first ones being producted during the 10-min annealing at 253 °C and the second ones during the subsequent cooling; small amounts of type L crystals are also obtained during this cooling. Surprisingly, if one increases the 253 °C annealing time up to 10 h, no significant increase of the relative proportion of type H crystals in the resulting sample is observed. The I-to-H reorganization is dramatically slowed down after a few minutes. This is a general behavior of PEEK oligomers, which has been discussed elsewhere.[11]

It is possible to isolate type I or type H crystals by appropriate crystallization conditions. However, we did not succeed in finding conditions leading only to the production of type L crystals. Mostly type I crystals are obtained after the crystallization procedure of Figure 4g. Type H crystals are obtained by crystallizing the oligomer from the molten state (270 °C) at high temperatures for long times (12 h at 250.5 °C; Figure 5a). If lower crystallization temperatures are selected, type I crystals are predominantly formed (30 min at 241.6 °C; Figure 5b). Finally, if the crystallization temperature is further reduced, the oligomer crystallizes dynamically as described above, to give a mixture of type I and type L crystals.

An interesting result is obtained when the virgin powder is "annealed" 10 min at 246 °C, i.e., just above the melting temperature of type I crystals, before being cooled to room temperature (Figure 5d). The melting endotherm corresponds neither to pure type I crystals nor to pure type H crystals but is located just in between the usually observed values. We ascribe this observation to the progressive transformation of type I crystals into type H crystals, leading to a species of intermediate character. The experiment shows that there is a continuous morphological path going from type I to type H crystals.

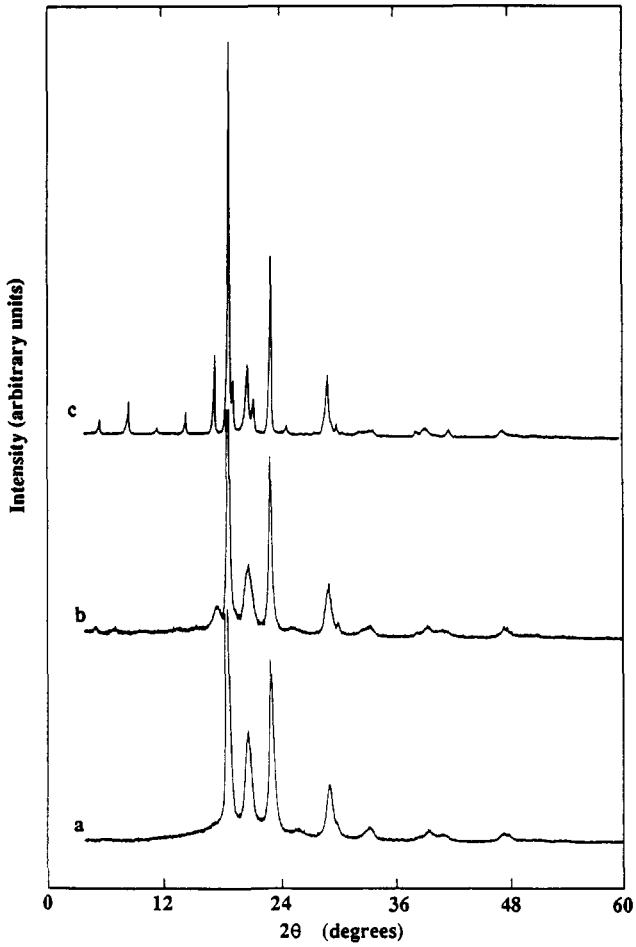

Figure 6. WAXS patterns of the virgin powders of (a) FK-(EEK)$_4$F, (b) EEK(EEK)$_1$EE, and (c) EEKEE. The patterns are similar to the polymer pattern, except for the presence of reflections due to the chain ends stacking in the smaller compounds.

Optical microscopy (OM) observations fully parallel DSC results in regards to multiple melting and the dramatic slowing down of the I-to-H reorganization rate. Various morphologies were observed by OM depending on crystallization temperature (see below); however, the different morphologies are not correlated to the existence of the different crystal types.

1.2. X-ray Scattering. WAXS Results. The powder patterns of the virgin powders of all the oligomers present great similarity with the PEEK patterns published in the literature.[12] Some representative examples are given in Figure 6. For the longest oligomers, FK(EEK)$_4$F and EEK-(EEK)$_2$EE (Figure 6a), the patterns are fully similar to that of the polymer, with four strong reflections: 110, 113, 200, and 213 (the indexing referring to the usual PEEK until cell[3-7]). For oligomers of intermediate length (FK(EEK)$_3$F and EEK(EEK)$_1$EE), the powder patterns are identical to the previous ones, except that small reflections are observed at low angles, due to the packing of the lamellae (Figure 6b). Finally, for still shorter oligomers (Figure 6c), small perturbations of the usual PEEK pattern are observed for 2θ angles higher than 18°, and numerous strong Bragg reflections appear at lower angles, giving evidence for the highly ordered lamellae packing. The lamellae thickness evaluated from these low-angle reflections is virtually identical to the computed extended chain length (Table V).

Experiments performed on oligomers in which the proportion of the various crystal types is modified by appropriate heat treatments (Table IV) give powder patterns identical to the virgin powders, except for slight changes in the values of the a and b lattice parameters (Table V). In all cases, these changes are smaller than 1.5%. From these observations, it can be safely concluded that the various crystal types observed by DSC are not due to different crystalline unit cells. However, the chain packing inside the crystals (a and b) lattice parameters) is slightly affected by the nature of the crystal type.

For phenoxy-ended oligomers, the chain packing is almost independent of the oligomer length. Moreover, variations in the dominating EEK(EEK)$_1$EE crystal type do not bring an important change in the chain packing (b decreases less than 0.7% and a increases less than 0.5% when going from ~25/75/0 to ~0/40/60 types L/I/H). The cell cross section is hardly affected, since a and b vary in opposite directions (less than 0.2% variation for the same case as above).

The behavior of fluoroaryl ketone-ended oligomers however is quantitatively different revealing the important influence of this end group. First, the longer the oligomer chain length, the higher b and the lower a. The first parameter decreases about 1.4% while the second increases 1.6% on going from FK(EEK)$_1$F to FK(EEK)$_4$F. However, the cell cross section remains constant within 0.2%. Second, when the proportion of the high-temperature melting crystal types is increased, a increases and b decreases in a much more pronounced manner than for the phenoxy-ended oligomers, but again the cell cross section remains almost constant.

1.3. X-ray Scattering. SAXS Results. The SAXS patterns of the shortest PEEK oligomers just show the first order of the Bragg reflections also detected on the low-angle side of the WAXS patterns (Figure 7a). The distances found by quoting the peak value of this first order agree with the previous WAXS determination within 0.08 nm, and usually better (Table VI); they are equal to the oligomer computed chain lengths (EEKEE, FK-(EEK)$_1$F, FK(EEK)$_2$F).

For longer oligomers (Figure 7), the SAXS pattern usually shows two Bragg reflections corresponding to distances (d_1 and $2d_2$) 3–6 Å larger than the computed extended chain lengths (Table VI). This is evidence for the existence of some chains protruding at the lamellae surface. The period of the lamellae packing is weakly sensitive to the proportion of the various crystal types. It tends to increase with the proportion of low melting type crystals (Table VI and Figure 7b–g). However, these variations are restricted to 2–3 Å only. Variations in the cooling rate from the melt affect also slightly the period of the lamellae packing, other things being constant.

A closer inspection of the SAXS patterns of the oligomers reveals for one sample (Φ_1/250C) the presence of supplementary reflections incommensurate with the main Bragg reflections. The SAXS pattern is shown at a larger scale in Figure 8 (type H crystals). Two significant smaller peaks are observed, corresponding to Bragg distances of 9.60 and 4.55 nm. The first of these peaks is observed in the original smeared pattern; the second one appears only after slit-width desmearing but is not due to amplification of statistical noise since it is preserved even after desmearing of a strongly smoothed original smeared pattern. It is particularly remarkable that the oligomer extended length (4.57 nm) corresponds to the Bragg distance of the second small peak.

Table IV
Description of the Oligomer Samples Analyzed by X-ray Diffraction

oligomer	sample name	thermogram ref[a]	thermal treatment[b]	crystal types composition
EEKEE			VP	c
EEK(EEK)$_1$EE	Φ_1/VP	Figure 2c	VP	~27/75 L/I
	Φ_1/253A	Figure 5c	VP + 10-min annealing at 253 °C	~40/60 I/H
	Φ_1/246A	Figure 5d	VP + 10-min annealing at 246 °C	intermediate between I and H
	Φ_1/250C	Figure 5a	crystallized from melt 12 h at 250.5 °C	H
	Φ_1/SC	Figure 3a	crystallized from melt at 10 °C min^{-1}	~50/50 L/I
	Φ_1/C/245S	Figure 4g	~previous sample + 2-min annealing at 245 °C	~I
EEK(EEK)$_2$EE			VP	c
FK(EEK)$_1$F			VP	c
FK(EEK)$_2$F			VP	c
FK(EEK)$_3$F	F_3/VP		VP	~25/75 L/I
	F_3/SC		crystallized from melt at 10 °C min^{-1}	I
	F_3/Q		air quenched from the melt	I
	F_3/310A		VP + 10-min annealing at 310 °C	~50/50 I/H
FK(EEK)$_4$F	F_4/VP		VP	L
	F_4/317A		VP + 50-min annealing at 317 °C	~60/40 L/H
	F_4/SC		crystallized from melt at 10 °C min^{-1}	L
	F_4/Q		air quenched from the melt	L

[a] Indicates the figure in which the 10 °C min^{-1} heating scan of the sample is presented, if any. [b] VP = virgin powder. [c] Compound having only one crystal type.

Table V
Unit Cell *a* and *b* Dimensions of the PEEK Oligomers

oligomer	sample name[a]	crystal types composition	a (nm)[b]	b (nm)[b]	ab (nm^2)	L_{measd} (nm)[c]	L_{comptd} (nm)
EEKEE			0.7687	0.5957	0.4579	3.06	3.10
	Φ_1/VP	~25/75 L/I	0.7712	0.5962	0.4598		
	Φ_1/253A	~40/60 I/H	0.7749	0.5923	0.4589		
	Φ_1/246A	intermediate between I and H	0.7703	0.5964	0.4595		
EEK(EEK)$_2$EE			0.7689	0.5964	0.4586		
FK(EEK)$_1$F			0.7550	0.6080	0.4590	2.66	2.72
FK(EEK)$_2$F			0.7582	0.6058	0.4593	4.19	4.19
	F_3/VP	~25/75 L/I	0.7646	0.6018	0.4601		
	F_3/SC	I	0.7665	0.5994	0.4594		
	F_3/310A	~50/50 I/H	0.7762	0.5952	0.4620		
	F_4/VP	I	0.7670	0.5996	0.4599		
	F_4/317A	~60/40 I/H	0.7787	0.5937	0.4623		

[a] The nomenclature is given in Table IV. [b] Computed from the 110 and 200 reflections. [c] For the shortest oligomers, small-angle Bragg reflections are observed above 6 °, allowing measurement of the chain end's repetition distance (L).

The regularity of the lamellae packing and the size of the lamellae stacks have been estimated by analyzing the line width of the Bragg reflections, using[13]

$$D_m\delta_n = 1/N + (\pi g n)^2 \quad (1)$$

where D_m is the mean value of the lamellae spacing, taken as the average of d_1 and $2d_2$, and n is the order of the diffraction peak whose full-width at half-maximum (fwhm) is δ_n. The g parameter is the relative standard deviation of the lamellae spacing around its mean value and N is the mean number of lamellae per stack. The formula strictly holds for Gaussian variations of lamellae spacing, which is a questionable hypothesis, and its use is clearly imprecise when only two diffraction lines are available; however, it has the advantage to convert into more intuitive parameters the information contained in the line widths. The estimations of N and g are given in Table VI. In some instances these parameters could not be determined for reasons detailed elsewhere.[11]

For similar crystallization conditions, the paracrystalline disorder (g) is smaller and the number of lamellae per stack higher, the shorter the oligomer. The standard deviation of the lamellae packing of EEK(EEK)$_1$EE is ~0.2 nm, i.e., a little less than half the distance between two successive ether bridges. It increases up to ~0.5 nm for FK(EEK)$_4$F, roughly the distance between two bridges in the chain. Hence, chain ends tend to be less regularly packed relative to (001) planes as the oligomer length increases. For a given oligomer, it is difficult to separate the influence of the crystal types proportion and of the crystallization conditions on the g-value. Indeed, longer crystallization times at higher temperatures are required to obtain the highest melting types. Such conditions evidently result in a smaller crystalline packing disorder (compare sample Φ_1/250C with other EEK(EEK)$_1$EE samples).

1.4. Discussion. Origin of Multiple Melting Endotherms. In the following discussion, we shall try to elucidate the origin of type H and I crystals, setting aside the origin of the L crystal type. This is because the L melting endotherm cannot be obtained by isothermal crystallization and only appears after dynamic crystallization (in solution or from the melt). It is thus most probable that the resulting crystal population corresponds to a disordered form. The reproducibility of its melting temperature results from the fact that type L crystals are always obtained from similar dynamic crystallization conditions. The very fast L-to-I reorganization also supports the attribution of the L endotherm to disordered crystals.

It is not easy to elucidate the nature of complex melting. Obviously, the H and I endotherms are not due to (a) random crystallographic disorder, since the melting temperatures of type I and H crystals are reproducible using quite different crystallization conditions (this does not rule out minor variations of the melting temperatures due to such a disorder); (b) existence of various crystallographic cells (polymorphs), since the WAXS powder patterns are insensitive to the actual crystal types composition of the oligomers, except for minor dimensional variations; (c)

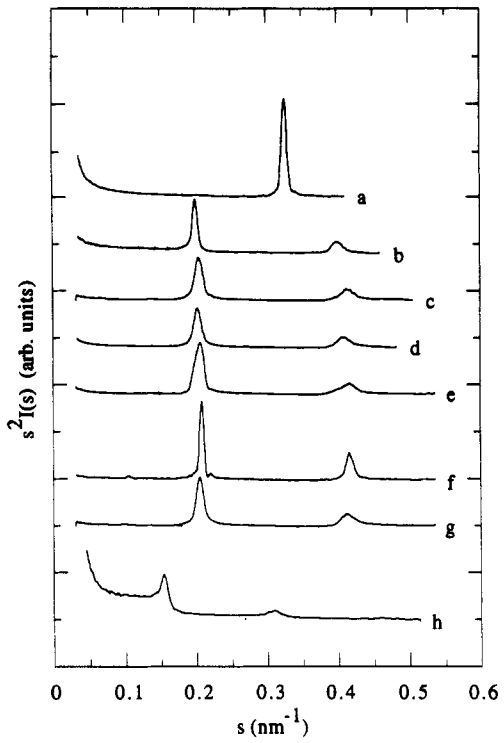

Figure 7. SAXS patterns of the phenoxy-ended oligomers. (a) EEKEE virgin powder. (b–g) EEK(EEK)$_1$EE; for a description of the samples, see Table IV: (b) Φ_1/VP, (c) Φ_1/253A, (d) Φ_1/246A, (e) Φ_1/SC, (f) Φ_1/250C, (g) Φ_1/C/245A). (All samples contain various proportions of the different crystal types.) (h) EEK(EEK)$_2$EE virgin powder.

chain folding, since the SAXS long distances are always equal to or higher than the oligomers extended chain lengths [besides, for such short compounds, chain folding is not expected (although the range of PEEK lamellae thicknesses quoted in the literature is limited to 2–6 nm[14–16])]; or (d) various inclinations of the chain-end planes versus chain axes, since this would also give rise to interlamellar distances smaller than the extended chain lengths.

At this point, it is necessary to recall essentials of theoretical results recently obtained by Abraham and Haworth.[9] These authors computed the interaction energies between PEEK chains in their usual crystalline packing, as a function of the relative placement of the bridging groups (i.e., the relative positions of the ether and ketone linkages of neighboring chains inside the crystal). It is common knowledge that the ether and ketone bridges are crystallographically equivalent;[8,17] however, Abraham and Haworth concluded that the most stable bridge placement in PEEK involves ketone bridge alignment in (100) planes, while the positions of these ketone "lines" in two successive (100) planes are staggered by at least one phenyl group. The situation is depicted in Figure 9a, for the EEK(EEK)$_1$EE case; the staggering gives rise to so-called staggered lamellae, in which all the chain ends are no longer aligned in planes. The surface free energy of such staggered lamellae is consequently higher than the surface free energy of the so-called eclipsed lamellae, in which all the chain ends are aligned in (001) planes (Figure 9b). However, according to Abraham, the bulk energy of the eclipsed lamellae is higher than the bulk energy of the staggered ones. One expects therefore for short oligomers the predominance of surface energy effects and thus eclipsed alignments of the bridges. As the oligomer length increases, bulk energy effects will compete with surface effects and staggered alignments become more probable.

The periods of the lamellae packing of the three shortest oligomers of this study, namely, EEKEE, FK(EEK)$_1$F, and FK(EEK)$_2$F, are equal to the computed extended chain lengths, confirming the adoption of eclipsed alignment by these oligomers. Since the interlamellar periods of the other oligomers are higher than their computed chain lengths, one is tempted to conclude that these oligomers adopt staggered alignments. However, this is clearly assailable, as a very small number of staggering defects in otherwise perfectively eclipsed lamellae would be sufficient to increase significantly the interlamellar period. From the increase of this period, it can only be concluded that at least some chains protrude from the lamellae. To determine whether this occurs regularly (staggered lamellae) or randomly (eclipsed lamellae with a few staggering defects) requires a deeper examination of the scattering curves.

Then the natural question arises whether or not the I and H crystal types identified by DSC correspond to staggered and eclipsed lamellae. For perfectly staggered lamellae, it can be expected that the protruding chains of one lamella will partly fit into the holes of the next lamella (Figure 10). The interlamellar distance between perfectly staggered lamellae will thus be only a little larger than the extended chain length. As for eclipsed lamellae, any staggering defect in this lamellae will increase the interlamellar distance of ~5 Å (Figure 10). On the whole, the situation is only slightly different from stacks of eclipsed lamellae with staggering defects (Figure 11a). The discrimination between eclipsed and staggered lamellae cannot be performed only on the basis of the measured mean interlamellar distances. Again, a full interpretation of the scattering curves is required.

We thus have attempted to simulate the SAXS patterns, using the kinematic theory of X-ray scattering. The intensity scattered by one stack of lamellae, with some packing disorder along the lamellae normal, can be computed for scattering vectors parallel to the lamellae normal (one-dimensional intensity):

$$i(s) = f_{lam}^2 \sum_{j,k=0}^{N} \exp\{2i\pi s(r_k - r_j)\} \qquad (2)$$

where r_j is the position of the jth lamella along the normal, $N+1$ is the number of lamellae in the stack, and f_{lam} is the Fourier transform of the projection onto the lamella normal of the electron density of one lamella, i.e., the one-dimensional structure factor. By averaging this expression for a large number of stacks, in which the probability to have r as the distance between two successive lamellae is $P_1(r)$ and is independent of the considered stack, one gets

$$i(s) = f_{lam}^2 \left[(N+1) + 2\,\mathrm{Re}\left\{ \frac{F^{N+2} - F^2}{(1-F)^2} + N\frac{F}{1-F} \right\} \right] \qquad (3)$$

with $F(s)$ being the Fourier transform of $P_1(r)$ and Re $\{x\}$ designating the real part of x. Note that, if N tends to infinity, the previous expression reduces to

$$i(s) = f_{lam}^2 (N+1)\,\mathrm{Re}\left\{\frac{1+F}{1-F}\right\} \qquad (4)$$

which is an expression found in standard textbooks.[18,19]

The scattering curve of sample Φ_1/250C (type H EEK(EEK)$_1$EE crystals) can be reproduced using expression (3) by assuming that this sample essentially consists of stacks of eclipsed lamellae with a very small number of staggering defects (Figure 11a). The real packing inside the majority of stacks can thus be approximated by a simple model (Figure 11b) in which perfect

Table VI
Results of the Analysis of the Oligomers SAXS Patterns

oligomer	sample name[a]	L_{comptd} (nm)	d_1 (nm)[b]	$2d_2$ (nm)[c]	δ_1 (nm^{-1})[d]	δ_2 (nm^{-1})[d]	N[e]	g[e]	suppl. refl. (nm)[f]
EEKEE		3.10	3.06 ● 0.02						
	Φ_1/VP		5.01 ● 0.02	5.00 ● 0.02	0.0087	0.0191	38	0.042	
	Φ_1/253A		4.88 ± 0.02	4.83 ± 0.02	0.0139	0.0219	18	0.036	
	Φ_1/246A	4.57	4.93 ● 0.02	4.90 ● 0.03	0.0131	0.0214	20	0.037	
	Φ_1/250C		4.81 ± 0.02	4.81 ± 0.01	0.0075	0.0126	36	0.029	9.60 ± 0.05 4.55 ● 0.02
	Φ_1/SC		4.85 ± 0.02	4.80 ● 0.02	0.0161	0.0245	16	0.037	
	Φ_1/C/245A		4.88 ● 0.02	4.85 ● 0.03	0.0124	0.0232	23	0.042	
EEK(EEK)$_2$EE		6.04	6.50 ± 0.02	6.46 ● 0.05					$3d_3$ = 6.53 ± 0.15
FK(EEK)$_1$F		2.72	2.66 ± 0.02						
FK(EEK)$_2$F		4.19	4.27 ● 0.05						
	F_3/SC	5.66	6.23 ● 0.04	6.18 ± 0.05	0.0130	0.0209	16	0.041	12.97 ● 0.1
	F_3/Q		6.37 ± 0.08	6.10 ● 0.15					
	F_3/310A		6.36 ± 0.05	6.25 ● 0.05	0.0245	0.0385	8	0.055	
	F_4/317A	7.13	7.67 ± 0.08	7.48 ± 0.1	0.0242	0.0342	6	0.051	
	F_4/SC		7.65 ± 0.08	7.45 ● 0.1	0.0186	0.0343	10	0.063	
	F_4/Q		7.87 ● 0.1	7.38 ● 0.15					

[a] The nomenclature is given in Table IV. [b] d_1 is the distance corresponding to the first-order Bragg peak. [c] $2d_2$ is twice the distance corresponding to the second-order Bragg peak. [d] δ_1 and δ_2 are the line widths (fwhm) corresponding to the previous Bragg peaks. [e] The mean number of lamellae per stack (N) and the paracrystalline disorder parameter of the lamellae packing (g) have been obtained by a simple line-width analysis. [f] Supplementary small reflection peaks are quoted in this last column.

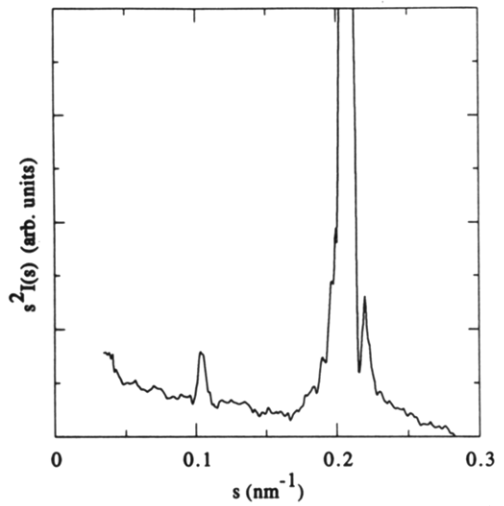

Figure 8. Expanded view of the SAXS pattern of EEK(EEK)$_1$EE type H crystals (sample Φ_1/250C), showing the presence of two smaller Bragg reflections.

eclipsed lamellae are placed randomly one over another, the distance between two successive lamellae being either r_1 (the thickness of an eclipsed lamellae) or r_2 (approximately 5 Å above the oligomer extended length). In this case

$$P_1(r) = p\delta(r-r_1) + (1-p)\delta(r-r_2) \quad (5)$$

with $\delta(r)$ the Dirac function. The structure factor of an eclipsed lamella (along the lamella normal) was calculated from the atom positions inside the cell, using crystallographic data published for PEEK[7] and atomic scattering factors equal to the number of electrons of the corresponding atoms, as only low s-values are considered. We fixed r_1 at 4.55 nm in accordance with the attribution of the corresponding small Bragg peak in the scattering pattern (Figure 8) to a small amount of stacks of perfectly eclipsed lamellae, without any staggering defects.

The measured and simulated scattering curves are presented in Figure 12. The agreement is satisfactory. The resulting parameters are physically significant, since r_2 (4.96 nm) is 4 Å higher than r_1 (one expects ~5 Å), N (32 lamellae per stack) is almost the same as that computed by the line-width analysis (36 lamellae/stack), and p (0.4) is high enough to accept the hypothesis that the number of defects per lamella is small.

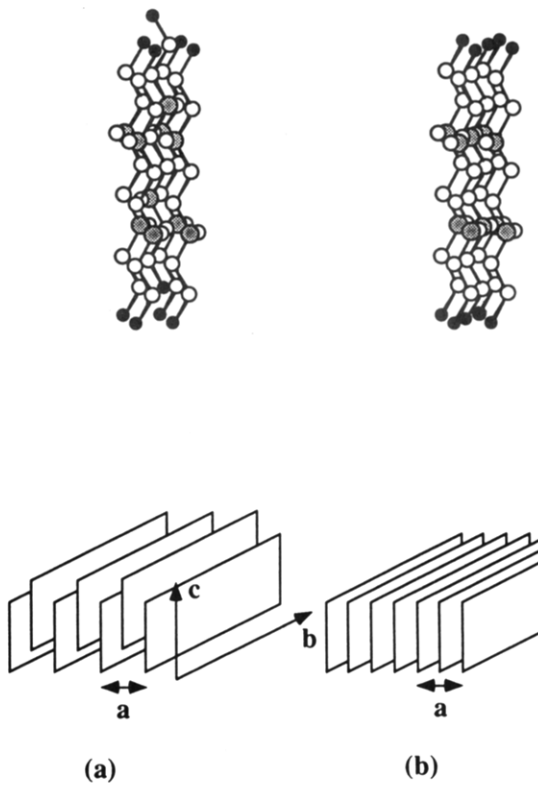

Figure 9. Unit cells (top) and schematic drawings (bottom) showing the relative disposition of (100) planes in the lamellae, for (a) staggered lamellae and (b) eclipsed lamellae of EEK-(EEK)$_1$EE. In the unit cell representations, only the bridging groups and the terminal H atoms are shown; the phenyl groups have been omitted for clarity. The staggered lamellae correspond to the PEEK most stable placement of ether and ketone bridges[9] (the schematic drawings exaggerate the staggering vector).

Moreover, one can also explain the presence of the small Bragg peaks corresponding to 4.55- and 9.60-nm repeating distance (Figure 8). As pointed out above, the first of these small peaks is due to a small amount of eclipsed lamellae stacks with no staggering defects and corresponds to the oligomer extended length within 0.2 Å. The second of these peaks arises from the existence of lamellae stacks wherein eclipsed lamellae without and with staggering defects regularly alternate. We have estimated the

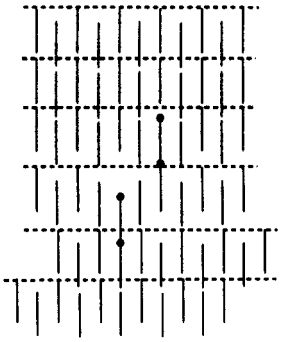

Figure 10. Schematic drawing of the packing of staggered lamellae with a few staggering defects (the staggering vector is exaggerated in this picture).

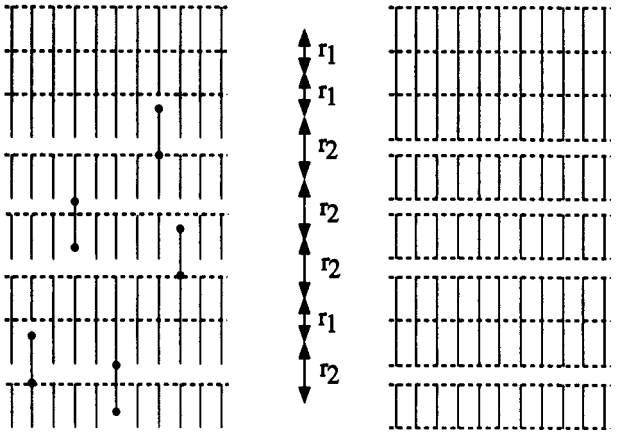

Figure 11. (a) Schematic drawing showing the way eclipsed lamellae with a small number of staggering defects pack into stacks. (b) Simple model used to simulate the real packing.

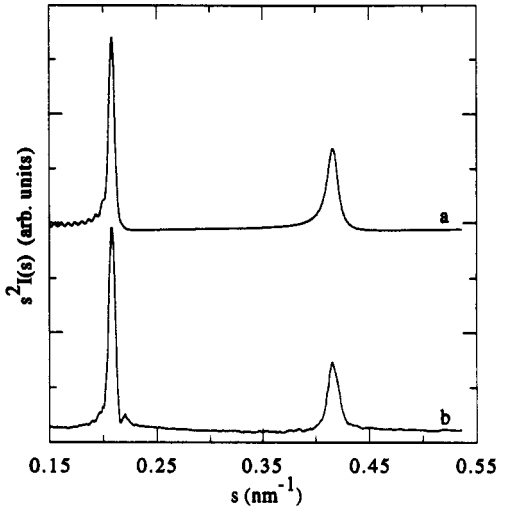

Figure 12. Simulated (a) and measured (b) EEK(EEK)$_1$EE type H crystals SAXS pattern (sample Φ_1/250C). The model is one in which eclipsed lamellae, some of them (~60%) having a small amount of staggering defects, pack into stacks of ~32 lamellae.

probability that a 32-lamellae stack has at least one regularly alternating succession of r_1 and r_2 distances, as a function of the length of this succession. Using the parameters obtained from the fit, i.e., lamellae stacks made of 13 (=0.4 × 32) r_1 distances and 19 (=0.6 × 32) r_2 distances, the probability to have at least one ($r_1/r_2/r_1/r_2/r_1/r_2/r_1/r_2$) regular succession in a stack amounts to ~7% (see the appendix). Such long regular successions will give rise to a Bragg reflection, located at ($r_1 + r_2$), i.e., 9.51 nm, which compares quite well with the measured value (9.60 nm).

Hence, we can safely conclude that EEK(EEK)$_1$EE type H crystals are eclipsed lamellae with a small number of staggering defects. Since the number of such defects per lamellae is small, the melting temperature of the lamellae will not be significantly decreased as compared to the perfect lamellae, and the DSC thermogram will exhibit one endotherm located at the melting temperature of perfectly eclipsed lamellae. However, the mean interlamellar distance is increased as already one defect is sufficient to cause an increase of the interlamellar distance. The lamellae packing is extremely sensitive to a small number of staggering defects.

We then attempted to fit the scattering curves of the EEK(EEK)$_1$EE sample predominantly consisting of type I crystals with the model described above, using the structure factors of staggered and eclipsed lamellae. The fits were not satisfactory, unless one modifies eq 3 to take into account differences in the interlamellar distance distribution from stack to stack:

$$i(s) = f_{lam}^2\left[(N+1) + 2\,\mathrm{Re}\left\{\int_0^1 B(p)\left(\frac{F_p^{N+2} - F_p^2}{(1-F_p)^2} + N\frac{F_p}{1-F_p}\right)dp\right\}\right] \quad (6)$$

In this equation, $B(p)$ is the probability to find a stack in which p is the probability that the distance between two successive lamellae equals r_1, and F_p is the Fourier transform of $P_1(p,r)$ (eq 5). This modification is required because the number of lamellae per stack is small for all EEK(EEK)$_1$EE samples except sample Φ_1/250C (cf. Table VI), and it is no more correct to consider each stack as equivalent to the others. With a proper choice of $B(p)$, it is possible to fit the results; however, the high number of adjustable parameters renders their physical significance questionable.

In order to reduce the number of adjustable parameters, it is necessary to measure samples for which $B(p)$ tends to a Dirac function. Such samples have to possess a large number of lamellae per stack and ideally as little disorder as possible. The realization of such samples requires slow crystallization, which occurs only at the highest crystallization temperatures, and invariably leads to the type H crystals. Hence, it seems hopeless to determine by SAXS the lamella type, staggered or eclipsed, corresponding to type I crystals.

However, all the experimental observations can be explained by postulating that type I crystals actually correspond to staggered lamellae with a small number of staggering defects. The reproducibility of the melting temperatures then results from the existence of well-defined eclipsed and staggered structures. The trend of the lamellae packing period to slightly increase when the proportion of lower crystal types increases is in accordance with the hypothesis. The increase of a and the decrease of b observed when the proportion of type H crystals is increased relative to type I crystals (Table V) is in agreement with Abraham's predictions.[9] According to these predictions, the passage from the most stable staggered bridge alignment (Figure 9a) to the eclipsed one (Figure 9b) would promote an increase of the distance between (100) planes (a lattice parameter); this increase could in turn allow for a slightly higher tilt angle between the phenyls and the (100) planes, which would result in a decrease of b. The evolution with oligomer length of the complex melting behavior for the phenoxy-ended series is also in agreement with the staggering hypothesis. The shortest oligomer does not exhibit complex melting and

adopt an eclipsed configuration. This is expected, since surface energy effects predominate over bulk energy effects for short oligomers. The longest oligomer does not exhibit complex melting; its lamellae packing distance is 5 Å higher than the computed extended length. One could thus accept that bulk energy now predominates over surface energy effects and that only a staggered configuration is accessible for this oligomer. The intermediate oligomer would then have surface and bulk energy effects of the same order. Hence, staggered and eclipsed lamellae will be formed depending on crystallization conditions, giving rise to the observed complex melting behavior. Finally, for this oligomer, one expects the existence of lamellae of intermediate nature, in which zones of dominant eclipsed character would coexist with zones having a dominant staggered character. The melting temperature of such an hybrid lamellae would be located somewhere in between the melting endotherm of the limiting pure lamellae. The existence of such an intermediate compound has been observed for a particular crystallization condition (sample Φ_1/246A). Hence, on the whole, the equivalence between type I crystals and staggered lamellae can be safely accepted.

Generally speaking, the fluoroaryl ketone-ended oligomers are less prone to interpretation due to their higher packing disorder. The *a* and *b* lattice parameters of these oligomers are more sensitive to changes in the crystal type than those of phenoxy-ended oligomers. From ^{13}C NMR results, it is known[2] that the carbon in the carbonyl group adjacent to the *p*-fluorophenyl is more deshielded than in carbonyl groups deeper along the chain. The dipole moment of this carbonyl end group is thus larger; this is the reason for the differences between the two oligomer types. The difference in the surface energy of the lamellae of both oligomer types also explains why the competition between bulk and surface energy effects still occurs for longer fluoroaryl ketone-ended oligomers than for phenoxy-ended ones (Table III).

At this point, an important conclusion of the present study can be derived. It is known[12,20] that the unit cell parameters of the PEEK polymer are strongly affected by changes in the polymer crystallization temperature (T_c). The main variations are observed for *a* and *b*, which both decrease when T_c increases. For instance, Wakelyn[20] reports for the PEEK polymer crystallized at 323 °C, as compared with the same polymer crystallized at 189 °C, a decrease of *a* of ~1.5% and of *b* of ~1.6%, which amounts to a cross-section decrease of nearly 3%. It has been argued[9] that this crystallographic density increase is due to variations in the relative placement of the ketone and ether bridges of neighboring chains. For low T_c, this placement would be disordered, with very few correlations between the relative positions of the ether and ketone bridges. With an increase of T_c, the placement would tend to a more stable alignment of the bridges, similar to the staggered lamellae described above. This would explain, following Abraham et al., the decrease of *a* and *b*.

However, for oligomers, the *a* and *b* variations due to the passage from eclipsed to staggered lamellae are significantly lower than those reported for the polymer with T_c. Moreover, for oligomers, the unit cell cross section is almost independent of chain staggering, any variation of *a* being counterbalanced by a variation of *b* in the reverse direction. Hence, the large unit cell dimensional changes observed for the polymer with T_c cannot be explained by the existence of staggering effects.

2. Crystal Morphology. In this section, we briefly present and discuss some of the morphologies observed for the oligomer crystals. As pointed out above, there is usually no important morphological variation between the different crystal types of a given oligomer, except for normal changes resulting from differences in the crystallization conditions. Hence, we shall strictly limit the discussion to elements relevant to a better understanding of the PEEK polymer. Complementary information of the oligomer morphologies can be found elsewhere.[11]

A typical structure obtained by crystallization from the melt is shown in Figure 13a. The morphology is polycrystalline, consisting of large monocrystalline grains, evoking typical metal micrographs; each grain appears differently colored in phase contrast, following its orientation. Initially, the grains are uncracked; however, upon cooling (to take photographs), numerous cracks appear. All the cracks are parallel inside a given grain; they actually indicate a direction perpendicular to the weakest crystalline forces in the crystals. As such, these cracks are thus of interest, since they provide some insight into the underlying disposition of the crystal unit cell.

In various instances, lozenge-shaped single crystals (Figure 13b,c) or truncated lozenges (Figure 13d) have been obtained. The cracks appearing after crystallization from the melt are almost parallel to the long diagonal, forming a ~40° angle with the lozenge faces. The angles between the cracks and the truncation planes are found to be 0 and 90°. These observations suggest that the cracks are parallel to (100) planes. Indeed, from the Bravais–Friedel law[21] the most prominent faces of the PEEK crystal are expected to be the (100), (010), and (110) faces. This is in agreement with experimental observations[22,23] showing mainly (110), (010), and (100) faces for PEEK lamellae. This also fits with the truncated lozenge-shaped single crystals observed for our oligomers. The Tracht of the oligomer crystals can be explained in terms of (110), (010), and (100) faces. From the oligomer unit cells, one expects an angle between (100) planes and (110) planes of ~37.5°. This corresponds fairly well to the angle measured between cracks and the lozenge faces of the $EEK(EEK)_2EE$ oligomer crystals (Figure 13c) or to the angle between the $EK(EEK)_3F$ longest faces and its inclined faces (Figure 13d).

Moreover, it has already been suggested by Lovinger and Davis,[22] on the basis of the chain zigzag arrangement inside the polymer unit cell, that the (100) planes are more susceptible to cleavage and misorientations. This has been illustrated by Tsuji et al.,[23] using high-resolution TEM: PEEK crystals have a misoriented structure with small-angle grain boundaries due to conjunction of successive edge dislocations having as probable Burgers vector (1/2)[100]. The greater weakness of cohesive forces between (100) planes as compared to (010) planes is also evidenced by the smaller variations of the *b* parameter. Hence, all these observations allow the identification of cracks with (100) planes.

For the longest oligomer crystallized at high crystallization temperatures (H_{F4} crystals of $FK(EEK)_4F$), spherulites are obtained. Figure 14 displays the morphologies obtained after 15 h and 30 min of crystallization at ~317 °C, followed by air quenching. The very fine texture is formed during the quench and allows us to discriminate very easily the structures formed during the isothermal crystallization. Interestingly enough, two types of spherulites are detected. The first ones, here after called R (for radial), are presented in Figure 14a. They are characterized by radial cracks, and well-defined Maltese crosses are observed between crossed polarizers. In the second type of spherulites, called T (for tangential), the cracks

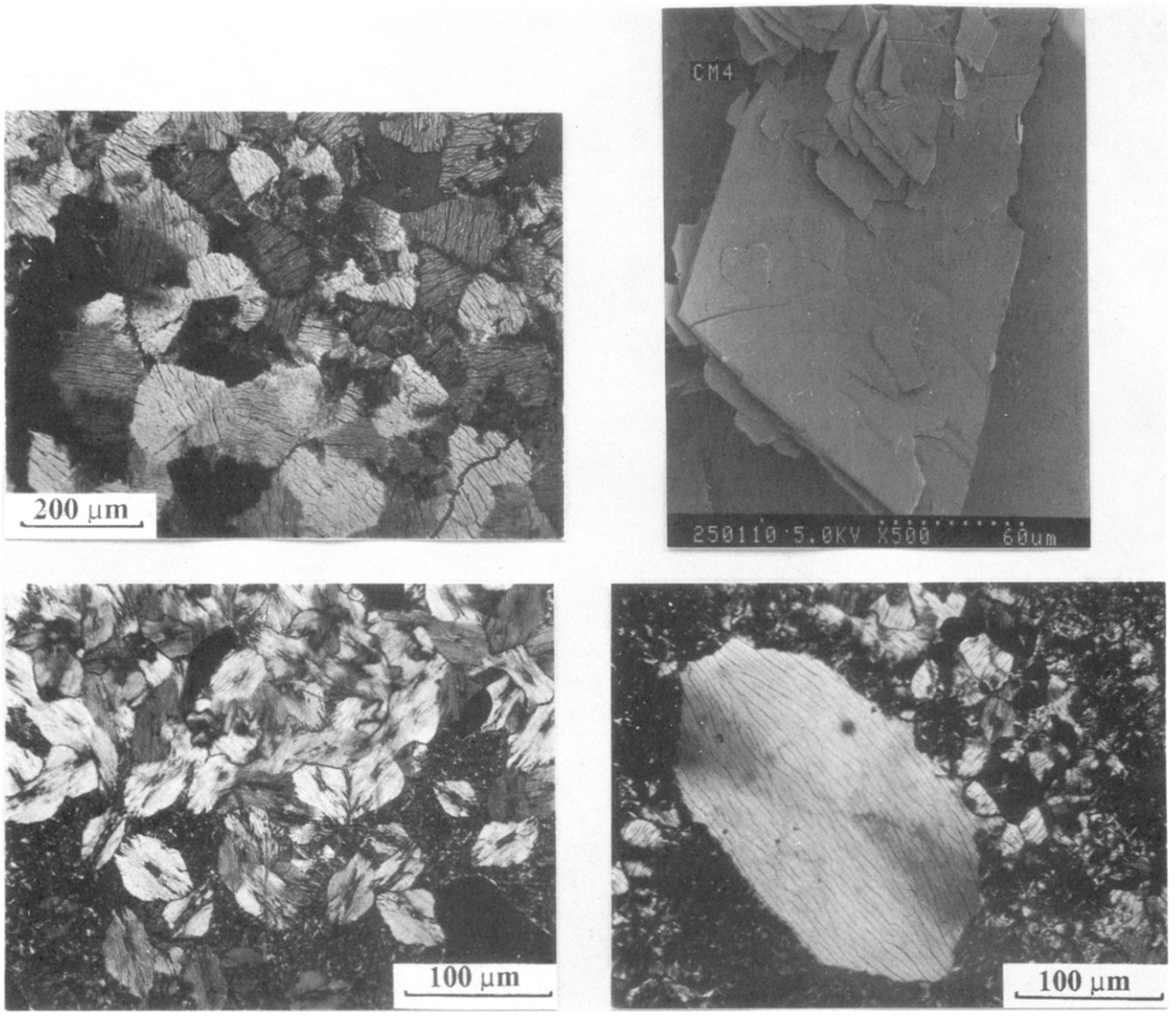

Figure 13. Representative examples of oligomer morphology. (a) Phase contrast optical micrograph showing the polycrystalline appearance of a 245 °C-crystallized EEK(EEK)$_1$EE sample (type I crystals). (b) Scanning electron micrograph of the FK(EEK)$_1$F virgin powder (lozenge-shaped single crystal). (c) Phase contrast optical micrograph of EEK(EEK)$_2$EE (lozenge-shaped structures obtained after 5 min of crystallization at 278 °C). (d) Optical micrograph (crossed polarizers) of FK(EEK)$_3$F (type I_{F3} single crystal obtained after 1 h of crystallization at ~310 °C).

are disposed circularly (Figure 14b,c). Although traces of a Maltese cross can still be detected in these spherulites, its intensity is much lower than for type R sperulites. Moreover, dark zones appear uniformly dispersed into these spherulites, corresponding to a homogeneous distribution of zero birefringence zones.

It should be noted that both spherulite types coexist in the same regions of the samples investigated; moreover, many spherulites are actually of mixed character, some of their sectors being of T type and others being of R type (Figure 14a). They both melt at the same temperature, revealing that they are both composed of H_{F4} type crystals.

Since the cracks have been demonstrated to be (100) planes in well-developed crystals, they will give precious crystallographic information for the spherulites, being perpendicular to the predominant *a*-direction. In type R spherulites, the cracks are radial; this indicates that *b* is mainly radial and *c* perpendicular to the view plane in these spherulites. The strong Maltese crosses observed between crossed polarizers for these spherulites point to a large spherulite birefringence, in accordance with a computation of PEEK refractive indexes (η) by Kumar et al.:[24] the result showed that η_b (1.48) is indeed much smaller than η_a (1.77) and η_c (1.97). The overall appearance of type R spherulites suggests that they are made of lamellae lying flat on each other, with crystallographic matching between each layer. They actually could be considered as single crystals growing from a central seed, with a huge number of edge dislocations having their Burgers vector parallel to [100].

In type T spherulites, the spherulites clearly cannot be considered as made of lamellae lying flat on each other. Moreover, (100) planes are tangential. Hence, the *a*-axis is predominantly radial in these spherulites. The *c*-axis is no longer parallel to the viewing direction; indeed, in such a case, one would expect spherulites with the same birefringence as R spherulites (except for the sign) and well-marked Maltese crosses. Hence, in this case one must admit that the *b* and *c* directions of the crystals adopt various angles relative to the view plane, depending on their position in the spherulite. From the results of Kumar et al.,[24] it can be derived that the PEEK optical axes lie in the *b*–*c* plane, forming ~34° relative to *b*. A zero birefringence dark zone will appear each time one optical axis is parallel to the viewing direction, giving rise to the much more jagged appearance of T spherulites in polarized light. A schematic drawing of the internal disposition of

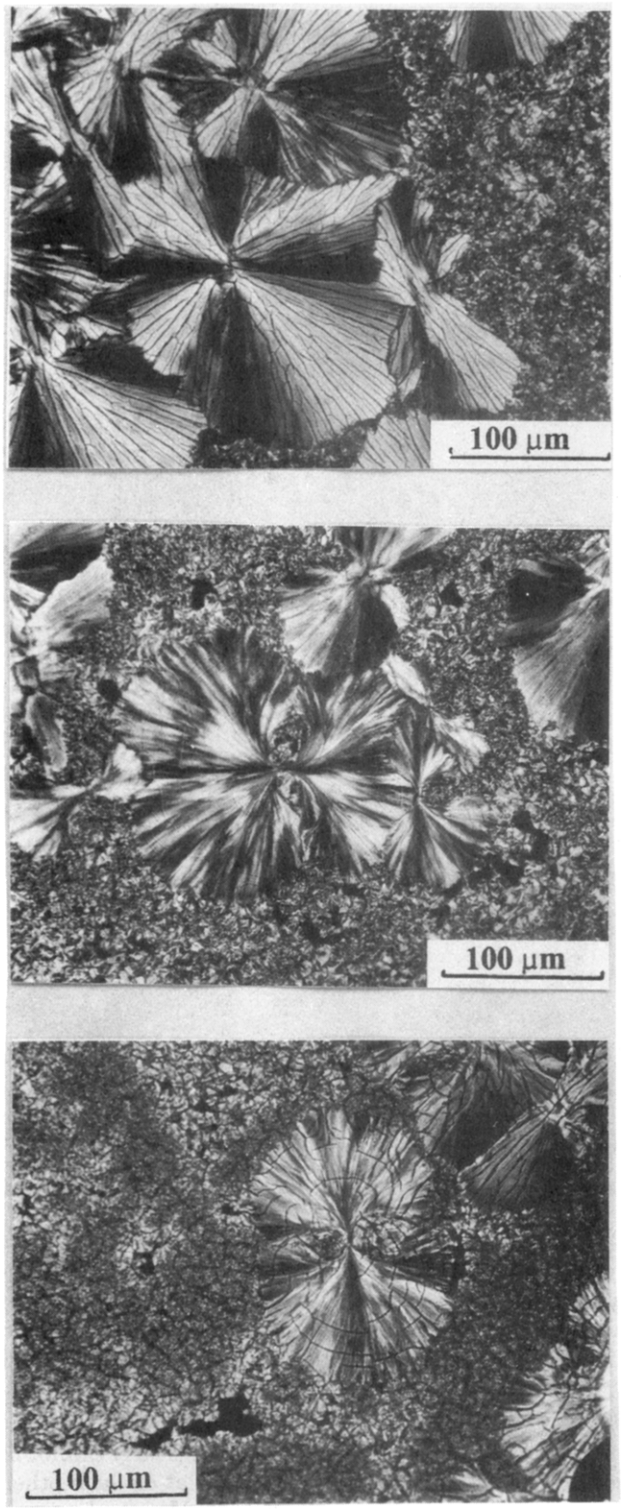

Figure 14. Optical micrographs (crossed polarizers) of FK-(EEK)$_4$F (type H_{F4} crystals), crystallized for 15 h and 30 min at -317 °C. (a) Type R spherulites. (b and c) Type T spherulites.

the unit cell inside both types of spherulites is given in Figure 15.

It has been claimed from all previous microscopic investigations on the polymer[22,23,25] that the *b*-axis is predominantly radial in PEEK spherulites and that the lamellae are elongated in the *b*-direction, because of preferred growth in this direction. Type R spherulites are in fair agreement with these observations. However, type T spherulites definitely disagree with them: their structure can be explained either by preferred growth in the *a*-direction, with rotation of the (*b*–*c*) planes along the

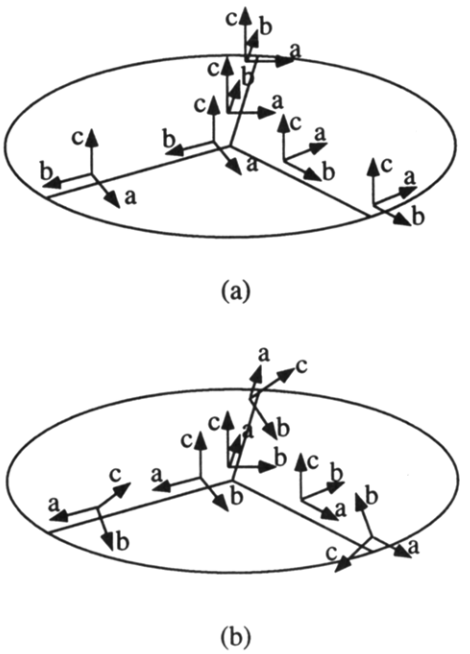

Figure 15. Schematic drawing illustrating the dominant internal disposition of the crystallographic axes inside type R (a) and type T (b) spherulites.

spherulite radius, or by cross-hatching,[26] i.e., formation of numerous lamellae perpendicular to the radial direction, growing on fewer radial lamellae (*b* being kept as the preferred growth direction). It is at the present time not clear why similar spherulites have not yet been observed for the polymer.

Conclusions

In the present work, structural and thermal analyses on PEEK monodisperse oligomers, having two different types of chain ends, are presented. On the experimental level, the following observations appear to be relevant for a better understanding of morphological, thermal, and optical aspects of PEEK:

1. Some oligomers exhibit complex melting as evidenced by reproducible multiple melting endotherms. The experimental observations can be explained by postulating the existence of various lamellae types, differing in the internal alignment of ether and ketone bridges, in accordance with the theoretical prediction of Abraham and Haworth.

2. Changes from eclipsed to staggered alignment of the bridges affect slightly the oligomer chain packing in the (*a*–*b*) plane. The effect is small for phenoxy-ended oligomers; it is stronger for fluoroaryl ketone-ended oligomers, due to a different value of the dipole moment of the terminal ketone.

3. The unit cell cross-section variation, on going from an eclipsed to a staggered alignment, is always much smaller than that reported for the polymer when its crystallization temperature is increased. Therefore, the polymer unit cell dimensional changes with T_c cannot be explained by changes of the isomorphic placement of ketone and ether bridges in the lamellae.

4. (100), (010), and (110) planes are stable oligomer crystal faces, in analogy with findings on polymer lamellae. (100) planes are prone to cleavage.

5. The longer oligomer of this study crystallizes into two spherulite types. In the first type (R), *b* is radial, *c* parallel to the viewing direction, and the birefringence is high. In the second type (T), *b* is predominantly tangential

and its orientation with respect to the viewing direction evolves along the spherulite radius; a lower birefringence results, with the presence of zones of zero birefringence dispersed into the spherulite. It is suggested that the morphology of such spherulites could be related to the presence of numerous cross-hatched lamellae.

It is striking to observe that short monodisperse PEEK oligomers, having well-defined chemical structures, present so many properties and challenges to interpretation. In view of this complexity, it is clear that at the present time one is still far from a full understanding of the polymer, taking into account its polydisperse character, its various chain-end nature,[27] its chain structure defects,[28] and its semicrystalline texture. Complementary work in the field of oligomers could contribute to this understanding.

The synthesis of longer *monodisperse* oligomers would be invaluable; however, it is not realistic to think that the synthetic route used to obtain the oligomers of this study will be able to lead to much longer compounds. New synthetic strategies have to be developed. Also, the postulated staggered/eclipsed nature of the oligomer lamellae should be confirmed by more precise techniques; atomic force microscopy could be of some help in this respect. X-ray structure determinations on single crystals could be attempted; however, the growth of the various crystal types in large monocrystalline assemblies is a prerequisite which will be difficult to fulfill. Computer modeling could bring some further insight into the problem, but this will not eliminate the need to resort to experimental practice to demonstrate the pertinence of computed models.

Experimental Section

Oligomer Synthesis and Characterization. Refer to paper 1 of this series.[2]

DSC. A Perkin-Elmer DSC2 was used throughout this work. Temperature was calibrated with indium and zinc for each of the scanning rates of this study, except for 50 °C min^{-1}, where the calibration performed at 20 °C min^{-1} was kept unchanged. Between 1- and 5-mg samples were used for each run. Unless otherwise stated, a new sample was taken for each run. Endothermic peaks were characterized by $T_{m,ons}$ (the intersection with the base line of the steepest tangent in the initial part of the peak) and $T_{m,peak}$ (the peak value of heat flux); the melting enthalpy, ΔH_m, was also computed. Exothermic dynamic crystallization peaks were characterized by their peak value ($T_{cc,peak}$), their onset value ($T_{cc,ons}$), and their crystallization enthalpy (ΔH_{cc}).

Optical microscopy was performed in polarized white light using a Zeiss Orthoplan-POL microscope. The crystal structures were observed between crossed polarizers or by phase contrast. A Mettler FP2 hot stage was used for all the compounds, except for FK(EEK)$_3$F and FK(EEK)$_4$F, for which a Stanton Redcroft hot stage was used.

WAXS. The recording of WAXS powder patterns was performed at 21 °C with a Siemens D500 diffractometer, equipped with a graphite secondary monochromator. The powder diffractograms were obtained between 6 and 60° (2θ), using Cu Kα radiation (1.5418 Å), with a scan rate of 0.5°/min. (2θ). The a and b cell dimensions were computed from the sharp 110 and 200 reflections, assuming an orthorhombic lattice as for PEEK. Computations taking into account the 113 and 213 reflections give essentially the same results.

SAXS. SAXS patterns were obtained at room temperature with a Rigaku rotating copper anode, operated at 7.5 kW (50 kV, 150 mA). Mark glass capillaries were filled with the oligomer powders and placed into an evacuated Kratky camera (slit collimation), having a slit width of 70 μm. The scattered intensity was recorded with a Braun PSPC, whose distance from the sample was ~30 cm. To calibrate precisely the sample-to-detector distance, the sharp first-order scattering peak of the EEKEE oligomer was fixed at s = 0.3266 nm^{-1}, corresponding to the value of the chain-end repetition distance computed from the five higher orders apparent on the WAXS pattern between 5 and 18°. From the PSPC channel width, the SAXS resolution was computed to be ~6.5×10^{-4} nm^{-1}. The background due to an empty capillary was recorded and subtracted from each sample measurement.

The smeared data were first desmeared to remove the slit-width effect, using the primary beam profile measured in the sample registration plane. The used routine was similar to the iterative method published by Glatter.[29] The width-desmeared curve was desmeared again to remove the slit-length effect. The procedure consists simply in solving the triangular system resulting from discretization of the convolution equation. It is known that by such a procedure the noise of the original curve is amplified in the desmeared curve. However, due to the high statistical quality of the width-desmeared original curve, this amplification was no problem. This simple procedure has the advantage of fully preserving the sharpness of the original Bragg peaks. All routines were written in Pascal and were run on a Macintosh II ci personal computer. Finally, a Lorentz correction was applied to the curves, since the scattering was obtained from isotropic powders. In this work, no attempt was performed to take into account the additional smearing due to the polychromaticity of the beam.

Acknowledgment. The authors are indebted to Dr. J. Naud for having performed the WAXS measurements on the oligomer powders, to Mrs. B. Vanderheyden for some help during the DSC studies, and to Mrs. M. Peeters for the kind sharing of her experimental practice on SAXS. A.J. expresses his thanks to the members of the Macromolecular Structural Chemistry Laboratory (Katholieke Universiteit Leuven) for having welcomed him during the SAXS measurements. Financial support from the Belgian National Fund for Scientific Research is gratefully acknowledged.

Appendix

Let us define the event A_n: there is *at least* one regular succession ($r_1/r_2/.../r_1/r_2$), r_1 occurring n times, in a stack of N lamellae comprising N_1 lamellae of thickness r_1 and N_2 lamellae of thickness r_2. We are searching the probability that such an event occurs: $P(A_n) = P_n$.

Define $A_{n,i}$ as the following event: there is such a succession in the stack, beginning at the ith lamellae. Then obviously

$$A_n = A_{n,1} \bigcup A_{n,2} \bigcup \dots \bigcup A_{n,N-2n+1}$$

From classical probability theory[30]

$$P_n = \sum_{i=1}^{N-2n+1} P(A_{n,i}) - \sum_{i=1}^{N-2n-1} \sum_{j=2+1}^{N-2n+1} P(A_{n,i} \cap A_{n,j}) + \sum_{i=1}^{N-2n-3} \sum_{j=2+1}^{N-2n-1} \sum_{k=2+j}^{N-2n+1} P(A_{n,i} \cap A_{n,j} \cap A_{n,k}) - \dots$$

Now

$$P(A_{i,n}) = \binom{N-2n}{N_1-n} \Big/ \binom{N}{N_1}$$

$$P(A_{n,i} \cap A_{n,j}) = \left[\begin{matrix} N-4n \\ N_1-2n \end{matrix}\right] \Big/ \binom{N}{N_1} \quad \text{for } 1 \le i \le N-4n+1 \text{ and } i+2n \le j \le N-2n+1$$

$$P(A_{n,i} \cap A_{n,j}) = \binom{N-(2n+(j-i))}{N_1-(n+(j-i)/2)} \Big/ \binom{N}{N_1} \quad \text{for } 1 \le i \le N-2n-1 \; i+2 \le j \le \min(i+2n-2, N-2n+1) \; (j-i) \text{ even}$$

$$P(A_{n,i} \cap A_{n,j}) = 0 \quad \text{elsewhere}$$

and so on. Numerical estimation of P_4 (for N = 32 and

$N_1 = 13$) leads to

$$P_4 = (3.26876 \times 10^7 - 1.00037 \times 10^7 + 2.87655 \times 10^6 - \sim 688\,787 + \ldots)/3.474 \times 10^8 = \sim 0.07$$

It should be stressed that this computation is only concerned with $(r_1/r_2/\ldots/r_1/r_2)$ successions, neglecting to count reverse successions $(r_2/r_1/\ldots/r_2/r_1)$ which will obviously give rise to the same peak corresponding to $(r_1 + r_2)$ Bragg distance.

References and Notes

(1) Research Assistant of the Belgian National Fund for Scientific Research.
(2) Part 1: Jonas, A.; Legras, R.; Devaux, J. *Macromolecules*, in press.
(3) Dawson, P. C.; Blundell, D. J. *Polymer* **1980**, *21*, 577.
(4) Rueda, D. R.; Ania, F.; Richardson, A.; Ward, I. M.; Balta Calleja, F. J. *Polym. Commun.* **1983**, *24*, 258.
(5) Hay, J. N.; Kemmish, D. J.; Langford, J. I.; Rae, A. I. M. *Polym. Commun.* **1984**, *25*, 175.
(6) Wakelyn, N. T. *Polym. Commun.* **1984**, *25*, 306.
(7) Fratini, A. V.; Cross, E. M.; Whitaker, R. B.; Adams, W. W. *Polymer* **1986**, *27*, 861.
(8) Blundell, D. J.; Newton, A. B. *Polymer* **1991**, *32*, 308.
(9) Abraham, R. J.; Haworth, I. S. *Polymer* **1991**, *32*, 121.
(10) The van der Waals radii of the terminal atoms were included in the computation of extended chain lengths ($r_F = 0.135$ nm, $r_H = 0.12$ nm). Bone lengths: C_{ar}–C_{ar}, 0.1395 nm; C_{ar}–H, 0.1084 nm; C_{ar}–F, 0.132 nm. Ring bond angle: 120°. *Handbook of Chemistry and Physics*, 54th ed.; CRC Press: Cleveland, OH, 1873). The bond lengths and angles of the ether and carbonyl bridges were taken from ref 9: C_{ar}–O, 0.1376 nm (C_{ar}–O–C_{ar}, 121.8°); C_{ar}–$C_{carbonyl}$, 0.1515 nm (C_{ar}–CO–C_{ar}, 121.3°C).
(11) Jonas, A. Ph.D. Thesis, Université Catholique de Louvain, 1992 (in English).
(12) Hay, J. N.; Langford, J. I.; Lloyd, J. R. *Polymer* **1989**, *30*, 489.
(13) See, e.g.: Hosemann, R. *Phys. Scr.* **1982**, *T1*, 142.
(14) Blundell, D. J.; Osborn, B. N. *Polymer* **1983**, *24*, 953.
(15) Blundell, D. J. *Polymer* **1987**, *28*, 2248.
(16) Cebe, P.; Chung, S. Y.; Hong, S.-D. *J. Appl. Polym. Sci.* **1987**, *33*, 487.
(17) Harris, J. E., Robeson, L. M. *J. Polym. Sci., Part B: Polym. Phys.* **1987**, *25*, 311.
(18) Balta-Calleja, F. J.; Vonk, C. G. *X-Ray Scattering of Synthetic Polymers*; Elsevier: Amsterdam, The Netherlands, 1989.
(19) Glatter, O.; Kratky, O. *Small Angle X-ray Scattering*; Academic Press: London, 1982.
(20) Wakelyn, N. T. *J. Polym. Sci., Part C: Polym. Lett.* **1987**, *25*, 25.
(21) Wunderlich, B. *Macromolecular Physics*; Academic Press: New York, 1973; Vol. 1.
(22) Lovinger, A. J.; Davis, D. D. *Macromolecules* **1986**, *19*, 1861.
(23) Tsuji, M.; Kawamura, H.; Kawaguchi, A.; Katayama, K. *Bull. Inst. Chem. Res., Kyoto Univ.* **1989**, *67*, 77.
(24) Kumar, S.; Anderson, D. P.; Adams, W. W. *Polymer* **1986**, *27*, 329.
(25) Waddon, A. J.; Hill, M. J.; Keller, A.; Blundell, D. J. *J. Mater. Sci.* **1987**, *22*, 1773.
(26) Norton, D. R.; Keller, A. *Polymer* **1985**, *26*, 704.
(27) Daoust, D.; Devaux, J.; Godard, P.; jonas, A.; Legras, R. In *Advanced Thermoplastics and Their Composites*; Kausch, H. H., Ed.; Carl Hanser Verlag: Munich, FRG, in press.
(28) Mullins, M. J.; Woo, E. P. *J. Makromol. Sci., Rev. Macromol. Chem. Phys.* **1987**, *C27*, 313.
(29) Glatter, O. *J. Appl. Crystallogr.* **1974**, *7*, 147.
(30) Feller, W. *An Introduction to Probability Theory and Its Applications*; 3rd ed.; John Wiley & Sons: New York, 1968; Vol. 1.